Journal of Ambient Intelligence and Humanized Computing
https://doi.org/10.1007/s12652-018-1026-6

ORIGINAL RESEARCH

Robust blood pressure estimation using an RGB camera

Xijian Fan[1] · Qiaolin Ye[1] · Xubing Yang[1] · Sruti Das Choudhury[2]

Received: 10 July 2018 / Accepted: 31 August 2018

Abstract
Blood pressure (BP) is one of important vital signs in diagnosing certain cardiovascular diseases such as hypertension. A few studies have shown that BP can be estimated by pulse transit time (PTT) derived by calculating the time difference between two photoplethysmography (PPG) measurements, which requires a set of body-worn sensors attached to the skin. Recently, remote photoplethysmography (rPPG) has been proposed as an alternative to contactless monitoring. In this paper, we propose a novel contactless framework to estimate BP based on PTT. We develop an algorithm to adaptively select reliable local rPPG pairs, which can remove the rPPG pairs having poor quality. To further improve the PTT estimation, an adaptive Gaussian model is developed to refine the shape of rPPG by analyzing the essential characteristics of rPPG. The adjusted PTT is computed from the refined rPPG signal to estimate BP. The proposed framework is validated using the video sequences captured by an RGB camera, with the ground truth BP measured using a BP monitor. Experiments on the videos collected in laboratory have shown that the proposed framework is capable of estimating BP, with a statistically compliance compared with BP monitor.

Keywords Remote photoplethysmograpy · Dicrotic notch · Gaussian curve fitting · Blood pressure estimation

1 Introduction

Blood pressure (BP) is an essential physiological parameter in the modern medicine. Standard BP monitoring apply the oscillometric technology (Drzewiecki et al. 1994), where the subjects need to wear sphygmomanometer device when measuring. Although it is easy to read and can provide accurate BP readings, it is incapable of obtaining continuous readings. Recently, many cuff-less BP measurements have been presented (Ma and Zhang 2005; Yoon et al. 2009), where pulse transit time (PTT), i.e., the time when a pulse signal passes between two different body parts, is detected for BP estimation. PTT can be estimated using either the time difference between electrocardiogram (ECG) and photoplethysmogram (PPG) (Gesche et al. 2012), or between two PPGs (Vanderpohl 2014). Most existing PTT based methods for BP measurement use contact sensor which is attached on the skin of people to obtain PPG or ECG.

Some studies using the contactless way for pulse estimation have recently proposed (Patzak et al. 2015). These contactless techniques are based on the similar physiological principles as contact PPG (cPPG) termed remote photoplethysmography (rPPG), which has been widely used for estimating various physiological parameters [e.g., pulse rate (PR) and respiration rate (RR)] (Malasinghe et al. 2017; Sathyanarayana et al. 2018). However, studies using rPPG to estimate PTT and the corresponding BP are very limited. To the best of our knowledge, only two methods (Jeong and Finkelstein 2016; Shao et al. 2014) attempt to use contactless way to detect PTT and BP. Jeong and Finkelstein (2016) use high speed camera to extract rPPG and estimate image-based PTT. Their study demonstrates that systolic BP has a higher correlation than image-based PTT. However, they use head and hand holder to prevent motion, which is impractical in real life as free movement should be allowed

✉ Xijian Fan
Xijian.fan@njfu.edu.cn

Qiaolin Ye
yqlcom@njfu.edu.cn

Xubing Yang
xbyang@njfu.edu.cn

Sruti Das Choudhury
S.D.Choudhury@UNL.edu

[1] Department of Computer Science, Nanjing Forestry University, Nanjing, China

[2] Department of Computer Science and Engineering, University of Nebraska-Lincoln, Lincoln, USA

Published online: 04 September 2018

in daily monitoring. Also, the cost of high speed camera is very expensive. Shao et al. (2014) estimate PTT between two rPPGs from face and palm regions. They introduce a tracking algorithm to handle the moderate movement in their experiments.

Both of the aforementioned studies adopt the traditional PTT estimation method used in cPPG, which directly estimate PTT using the maximum peaks over each waveform pulse and use the time interval of two detected peaks within the same cardiac pulse to define the PTT. This strategy has been proven efficient for PTT estimation in cPPG as the cPPG signals are relatively stable and robust against motion artifacts. However, they ignore the fact that the shape of waveform between rPPG and cPPG is slightly different although they share similar principle. When extracting rPPG waveform, rPPG signal suffers from slight movement between the subject and camera. Motion-induced distance change might distort the rPPG waveform, and accordingly impact the signal quality. Some important physiological features [e.g., dicrotic notch or diastolic peak (i.e., secondary peak)] arising in cPPG disappear in rPPG signal (shown in Fig. 1). The disappearance of the diastolic point will affect the main peak in terms of the location and shape, which further impacts PTT estimation. Since the PTT and BP are strongly related, the inaccuracy in PTT measurement could affect the performance of BP estimation.

To overcome the aforementioned existing problems in rPPG, we develop an adaptive Gaussian model to fit the original rPPG signal. By employing this model, the disappeared secondary peak can be revealed, and the actual main peak related to PTT can also be detected. It is the first time to construct parametric model for rPPG signal.

In this context, we propose a novel method to estimate PTT and BP using remote measurement. Firstly, we divide large face and palm ROIs into local region pairs for rPPG extraction, and then propose an algorithm to adaptively select the pairs which are suitable for PTT estimation. After that, we develop an adaptive Gaussian model to fit the typical rPPG waveform having the capability of revealing the disappeared features in rPPG. These features are useful for improving the PTT estimation.

Our contributions are summarized as follows:

- We develop a novel framework for remote PTT, and use a remote camera for the first time to evaluate both systolic and diastolic BP.
- We develop an adaptive selection strategy using frequency and temporal thresholding to obtain reliable rPPG pairs which have good shape and strength.
- We develop an adaptive model to fit the rPPG waveform. The PTT obtained from the fitted model shows improved accuracy.

2 Related work

2.1 Remote PPG

Remote photoplethysmography is an emerging research topic in the biomedical community and several studies have been proposed to estimate rPPG. Verkruysse et al. (2008) attempt to extract rPPG waveform under the condition of ambient light, where a normal RGB camera is used in their work. Poh et al. (2010) and Lewandowska et al. (2011) select

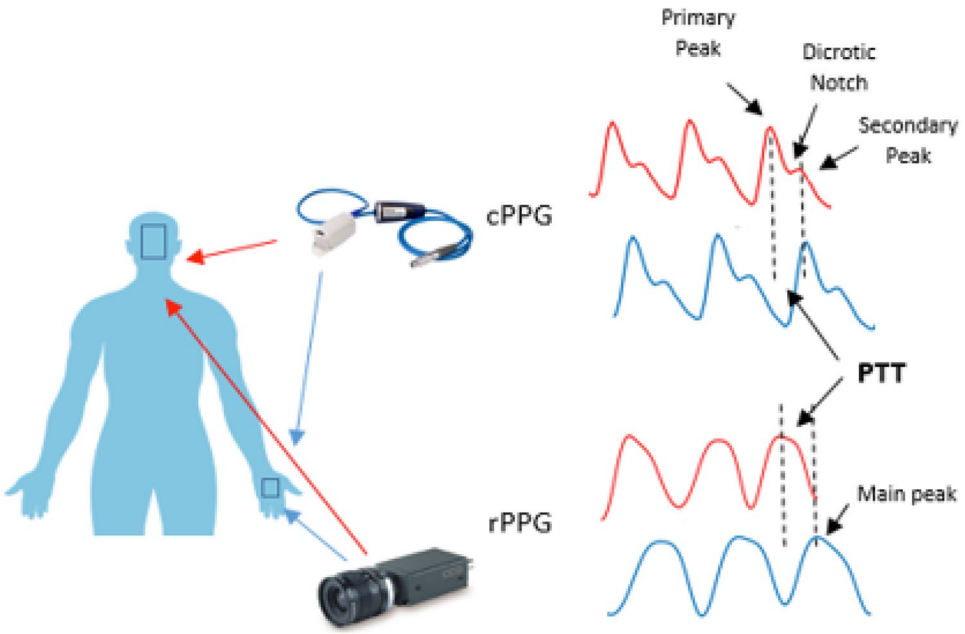

Fig. 1 Several characteristic parameters of PPG (i.e., rPPG and rPPG) and the PTT between two PPGs of different body parts

the whole face region to capture rPPG, where they apply independent component analysis (ICA) and principle component analysis (PCA) to estimate rPPG, prospectively. De Haan and Jeanne (2013) construct the physical model based on the color difference to obtain rPPG signal, improving the robustness of rPPG extraction. Li et al. (2014) propose a robust framework to extract rPPG, which can deal with the situation of illumination changes and motion variation. Recently, Tulyakov et al. (2016) utilize matrix completion method to extract rPPG, which is robust to estimate heart rate. Haque et al. (2016) propose a BCG based heart rate estimation approach by fusing corner feature points of good features and 49 predefined facial landmarks. Hsu et al. (2017) present a deep learning framework to estimate heart rate based on the time–frequency representation, achieving a good performance. Hassan et al. (2017) provide a comprehensive review for heart rate estimation based on facial video. Most of these rPPG techniques are applied to evaluate physiological parameters e.g., HR and RR.

2.2 PTT based BP estimation

Originally, PTT is defined as a time difference between two consecutive sites along the arterial tree when the arterial pulse traveling (Smith et al. 1999). ECG R wave and fiducial points of contact PPG waveform are regarded as the beginning and the ending to measure PTT (Ma and Zhang 2005; Jeong and Finkelstein 2012) prospectively. Recently, some researchers define PTT as time difference between two PPG waveforms from PPG sensors (Smith et al. 1999). These methods require placement of body-worn sensors. There are few studies on PTT estimation in a contactless way (Jeong and Finkelstein 2016; Shao et al. 2014). They compute the PTT between rPPGs from face. However, their methods are not robust to head motion, and the obtained PTT is not accurate due to the lack of analysis of rPPG characteristics.

Pulse transit time has been reported to highly relate to blood pressure and can be regarded as an indirect metric for the estimation of blood pressure (Mukkamala et al. 2015). The correlation between PTT and BP can be represented using physical models and empirical regression (Mukkamala et al. 2015). Linear, quadric and exponential regression are used for BP estimation (Gesche et al. 2012). In this context, we propose to estimated PTT from extracted rPPG signals, and then estimate systolic BP and diastolic BP with an initial calibration process.

3 Methods

Our framework consists of four main modules as shown in Fig. 2: (1) ROI tracking and sub-region division; (2) pair filtering; (3) rPPG modeling; and (4) BP estimation. In the first step, facial landmarks detection and tracking are applied to cope with two types of motions including rigid and non-rigid movements, reducing motion artifacts both in face and palm. After region division, small face and palm sub-regions are obtained. The process of division is to alleviate the phase shift resulting from large ROI. rPPG is then extracted over each sub-region pairs to form rPPG pairs. In the second module, in order to filter out reliable pairs, pair filtering is used to remove the signals which have poor quality in terms of both shape and strength. In the third module, an adaptive Gaussian model is applied to fit the rPPG waveform. After modeling, several characteristic parameters of rPPG are revealed, which can improve the PTT estimation. PTT is obtained from fitted rPPG, and then used to estimate BP. Figure 2 gives an overview of our proposed method.

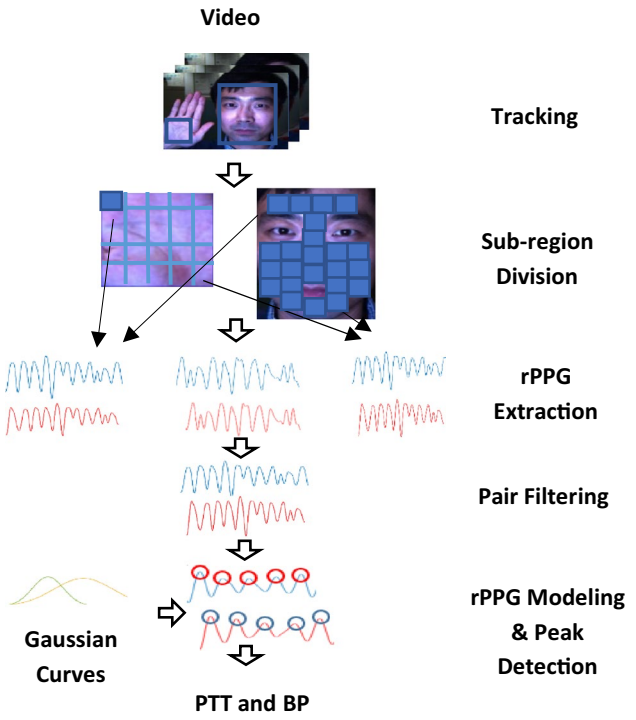

Fig. 2 Proposed framework for BP measurement from face and palm video

3.1 Region selection and tracking

Motion artifacts are inevitable in rPPG acquisition, which could confuse the changes resulting from physiological activities (i.e., color change due to blood flow) and skin shift. Thus, we employ two tracking algorithms to adaptively track the face and palm ROIs in order to compensate for rigid head and hand movements. OpenFace toolkit has been recently proposed (Baltrušitis et al. 2016), which is applied to localize the 67 facial landmarks, and then track the landmarks during successive frames. In our work, we do

not track the whole ROIs. Instead, we track a series of fiducial points, and construct a group of equal sized local regions according to the position of selected points. The strategy of local region selection aims to exclude face parts that have severe artifacts (e.g., blinking artifacts caused by eye).

Kernelized correlations filters (KLT) (Henriques et al. 2015) is used to track the ROI of palm due to its high computational efficiency and accuracy. The tracked palm ROI is aligned and also divided into a group of local regions of equal sizes.

After tracking, local regions from face and palm are combined to form a group of local region pairs. It is impractical to build pairs using the sub-regions from the same ROI (e.g., face), as the distance between such sub-regions is short resulting in extremely small time difference (e.g., below 10 ms). Only very high-speed camera can detect such time variance due to its relatively high temporal resolution. Thus, we only select pairs from two different ROIs.

3.2 PTT estimation

3.2.1 rPPG extraction

The chrominance-based method (De Haan and Jeanne 2013) is adopted to extract rPPG signal over each local region pair. We average the intensities both in green and red channels I_g and I_r from the selected regions over each frame, and then normalize them using the average $\mu(I_g)$ and $\mu(I_r)$ over a time interval as,

$$rPPG = \frac{\frac{I_g}{\mu(I_g)}}{\frac{I_r}{u(I_r)}} - 1. \tag{1}$$

The rPPG pairs are formed in this step.

3.2.2 Pair filtering

Pulse transit time can be estimated from two rPPGs over each formed rPPG pair. However, not all rPPG pairs are suitable for PTT estimation. rPPG signals of poor qualities should not be taken into account for PTT estimation. There are two factors resulting in bad rPPG: (a) the power of rPPG signals is different in each local region due to the vessel distribution and often results in very weak rPPG, which is regarded as a bad rPPG; and (b) the rPPG signal might be affected by motion artifacts caused by face anger change. For example, when facing only one light source, some face regions e.g., nose will result in shadow on face skin. Motion will accordingly change the intensity in certain face local regions. The rPPG signals affected by such motion artifacts are also regarded as bad rPPG.

In PTT estimation, we need to remove the rPPG signals which are regarded as bad. Thus, we propose an adaptive algorithm to remove the pairs that contains the rPPG with bad quality.

A goodness metric based on the signal-to-noise ratio (SNR) is utilized to qualify the quality of rPPG (Kumar et al. 2015). The goodness metric involves the strength of rPPG signal extracted from local regions and the corresponding noise power. We also apply the goodness metric for evaluating the quality of rPPG pairs.

Given an rPPG pairs $P = [S_{FR}, S_{PR}]$, goodness metric g can be defined as

$$g = f(S_{FR}) \cdot f(S_{PR}) \tag{2}$$

where $f(\cdot)$ is SNR estimation, which is defined as

$$f(S) = \frac{\sum_{f_{HR-r}}^{f_{HR+r}} \hat{S}(f)}{\sum \hat{S}(f) - \sum_{f_{HR-r}}^{f_{HR+r}} \hat{S}(f)} \tag{3}$$

where $\hat{S}(f)$ is the Fourier transform of S, f_{HR} denotes the estimated heart rate, r denotes the small range in the Fourier frequency, and $[f_{HR} - r, f_{HR} + r]$ denotes a small range near the estimated heart rate.

The pairs having small value of goodness metric show lower strength, which are rejected. A series of pairs are filter out by using thresholding function. Due to the motion artifacts, the shape of some cycles in rPPG is disturbed, resulting in a shift of peak. The goodness metric analysis based on frequency domain could not reflect this phenomenon. In some case, the pairs which have large goodness metric are still not reliable from the perspective of time domain. Take a rPPG pair for example, the peak over each cycle in face rPPG should be detected in earlier position than in palm rPPG (denoted in red), as the pulse wave arrives at face earlier (shorter distance from heart) than palm. However, the peak of face rPPG falls behind that of palm rPPG in some cycles due to the motion artifacts. These cycles are regarded as unreliable cycles and rPPG have a certain number of such unreliable cycles is regarded to be unreliable, which needs to be removed. Figure 3 shows an unreliable rPPG pair but having good SNR.

An adaptively selection strategy is applied to remove the unreliable rPPG pairs. Based on the empirical criteria that PTT between face rPPG and palm rPPG ranges from 10 to 60 ms (Jeong and Finkelstein 2016; Shao et al. 2014), the detected peak difference in one cycle from rPPG should be within this range. Only the cycles which have the correct peak difference can be selected as reliable cycles. We select rPPG pairs which have sufficient number of reliable cycles as reliable pairs, where the unreliable pairs are cancelled out after applying this strategy. Among these reliable rPPG pairs, the rPPG pair which has the highest goodness metric is finally selected.

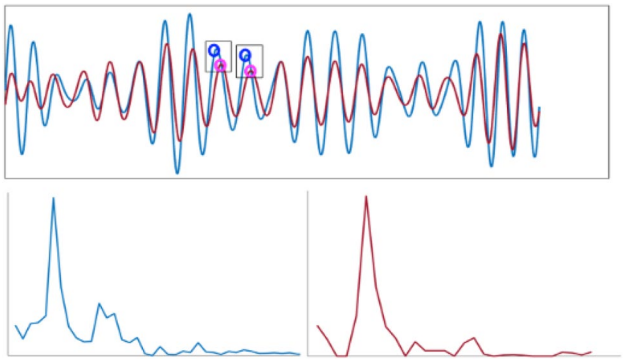

Fig. 3 Unreliable pairs have good SNR. The upper sub figure shows two signals in time domain with incorrect peak locations, while the bottom two sub figures shows the frequency domain of two signal. Black box denotes the correct peak difference (reliable cycle) over a period of cycle

3.2.3 Modeling rPPG

The secondary peak is often buried into the main peak (shown in Fig. 4) which affects the location and amplitude of the main peak. This is called peak shift phenomenon. It means that the main peak visibly appearing in the rPPG is not the actual peak position. Thus, directly using main peak to estimate PTT will result in an inaccurate value.

In order to obtain more accurate PTT, it is crucial to localize the actual peaks of rPPG. The position of secondary peak can be used to estimate the actual peak (Martín-Martínez et al. 2013). Thus, we aim to reveal the buried secondary peak to obtain the actual peak in rPPG.

Given the nature of the PPG signal, Gaussian curves are employed to model the cPPG (Martín-Martínez et al. 2013). Due to the similar principle between cPPG and rPPG, we employ the Gaussian curves to model the rPPG signal. Figure 4 shows the two Gaussian curve models for fitting rPPG and cPPG. The figure clearly shows the peak shift phenomenon in rPPG.

Since the original rPPG signal is formed resulting from the superposition of two waves including one forward and one backward, we construct an adaptive Gaussian model (AGM) consisting of two Gaussian curves to model the rPPG as,

$$S = \sum_{K=1}^{2} A_k \exp\left[-\frac{(t-\mu_k)^2}{2\theta_k^2}\right] \tag{4}$$

where θ_k is the standard deviation, μ_k is the mean, and A_k is the amplitude. The parameters of this gaussian model are computed using the means of a least square minimization:

$$\sum_{j=1}^{N} \left(\text{rPPG} - S_j\right)^2 \rightarrow \min . \tag{5}$$

The rising part of the main peak of rPPG signal only relies on heart rate, and is not affected by reflect wave (Rubins 2008). Therefore, we adopt the values of mean and the standard deviation according to the location and the shape of the rising part of the main peak. Then, we adjust the amplitude of the fitting curve based on the amplitude of the main peak of the original rPPG signal. Finally, we subtract the fitted curve from the original rPPG to get the secondary peak of the adjusted rPPG signal. AGM fitting is shown in Fig. 5, which shows the first Gaussian curve fits the rising part of the first peak. The secondary peak is obtained, and the problem of peak shifting is clearly displayed.

3.3 BP estimation

An empirically determined nonlinear function calibrating PTT and BP was applied for our BP estimation, and SBP can be estimated through the following Eq. (5).

$$\begin{aligned} SBP_{\text{PTT}} = {} & P1 \times PWV \times e^{(P3 \times \text{PWV})} + P2 \times PWV^{P4} \\ & - \left(\text{SBP}_{\text{PTT},cal} - SBP_{cal}\right) \end{aligned} \tag{6}$$

where $P1$, $P2$, $P3$, and $P4$ are empirically determined parameters, $SBP_{\text{PTT},cal}$ denotes the estimated SBP using PTT, and

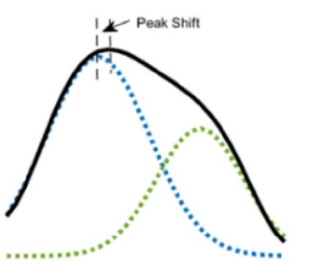

Fig. 4 Two-Gaussian-curve model for fitting rPPG (left) and cPPG (right)

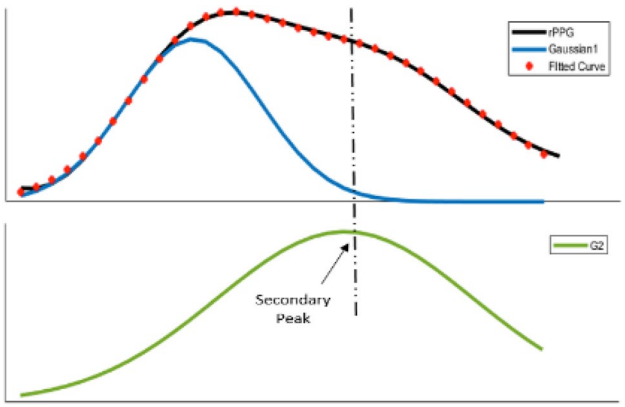

Fig. 5 Secondary peak detection using adaptive Gaussian fitting

SBP_{cal} denotes the SBP obtained by a BP monitor from a calibration procedure. Thus, DBP can be estimated i.e.,

$$DBP = SBP - \mathrm{PP}_0 \cdot \left(\frac{\mathrm{PTT}_0}{\mathrm{PTT}}\right)^2 \tag{7}$$

where PP denotes pulse pressure and the subscript 0 are those obtained from a calibration procedure.

4 Experiments

4.1 Datasets

Since there is no publicly available dataset for remote BP estimation, we introduce a benchmark dataset 'VideoBP' to evaluate the proposed BP estimation method. We used a RGB camera to capture 24-bit color videos at 120 frames per second (fps) with the size of 640 × 480. At the beginning of experiments, the reference BP including SBP and DBP were measured by commercial BP monitor (Omron HEM-6121). Subjects sit still and raised their right hands just beside the face to assure the camera capture face and palm region. Six subjects aged from 20 to 35 were enrolled. All videos were then analyzed including localizing ROI regions, tracking, extracting rPPG and estimating PTT and BP in Matlab.

Vicar dataset (Tasli et al. 2014) is used to evaluate the performance of the our secondary peak detection method and PTT estimation method in rPPG. In this dataset, the ground truth cPPG is provided and synced with the captured video. Ten subjects aged from 20 to 35 are involved for recording. The recorded videos have the size of 720 × 1280 with 30 fps, and an average duration is 90 s. A CMS-50 Pulse Oximeter is attached on the subject's fingertip for the ground truth pulse signal (i.e., cPPG). In our experiment, cPPG and video are interpolated to 256 HZ.

4.2 Validation of secondary peak detection

The proposed method of secondary peak detection using AGM fitting is validated in this experiment. A characteristic feature of normal PPG is introduced for evaluation, which is systolic (primary) peak to diastolic (secondary) peak time (SDT). The SDT relates to the time from heart to periphery and back. Vicar dataset is used in our experiment. The ground truth SDT (GT-SDT) is directly computed based on the location of primary and secondary peak from the ground truth cPPG. We extract rPPG signal from the face video, and then use AGM to detect the location of secondary peak and adjusted main peak. The detected two peaks are used to compute SDT (AGM-SDT). The SDT performance of ground truth cPPG and rPPG using proposed AGM are shown in Table 1, which shows there is slight variation between ground truth and rPPG in SDT. It means that our method is able to detect the invisible secondary peak effectively.

Table 1 Mean (standard deviation) SDT of ground truth cPPG and rPPG using proposed AGM

	GT-SDT	AGM-SDT
1	0.48 (0.006)	0.43 (0.010)
2	0.42 (0.009)	0.47 (0.012)
3	0.46 (0.007)	0.47 (0.008)
4	0.40 (0.015)	0.46 (0.010)
5	0.51 (0.010)	0.55 (0.014)
6	0.52 (0.009)	0.51 (0.010)
7	0.48 (0.011)	0.49 (0.013)
8	0.42 (0.004)	0.46 (0.008)
9	0.44 (0.025)	0.48 (0.034)
10	0.52 (0.011)	0.50 (0.011)
Mean	0.47 (0.040)	0.48 (0.033)

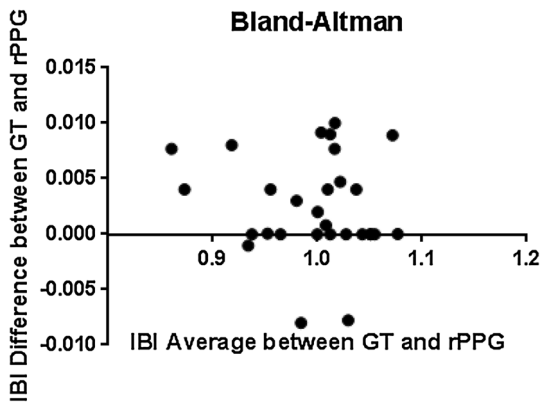

Fig. 6 Bland–Altman plot of IBI between ground truth cPPG and rPPG

Interbeat interval (IBI) defined as the interval between successive main peaks is also used to validate the adjusted main peak. Bland–Altman plot of IBI between ground truth cPPG and rPPG of subject 1 in Vicar dataset is presented in Fig. 6, showing the correlation between the IBIs of cPPG and rPPG. The adjusted main peak using the proposed method in rPPG can be an alternative way to detect IBI due to its accuracy.

4.3 Validation of adjusted PTT

VideoBP dataset is used for the validation of adjusted PTT using AGM. We estimate the adjusted PTT using AGM and the original PTT without using AGM in VideoBP dataset, and compute their R^2 values with the reference BP. Figure 7 shows the R^2 values between the PTT and BP both using AGM and without using AGM. It is obvious that PTT using

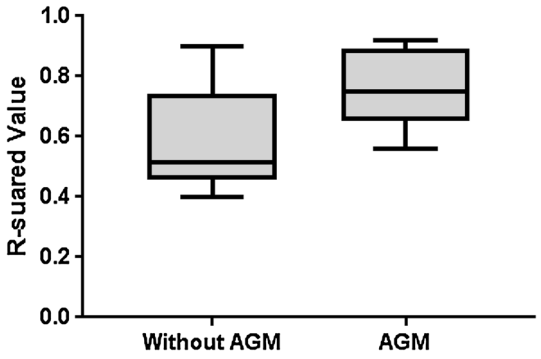

Fig. 7 R^2 values between PTT and BP using AGM and without using AGM

Table 2 Correlation between PTT and SBP/DBP

	Correlation r	
	SBP	DBP
1	−0.732	−0.804
2	−0.832	−0.767
3	−0.690	−0.543
4	−0.943	−0.567
5	−0.961	−0.629
6	−0.879	−0.683

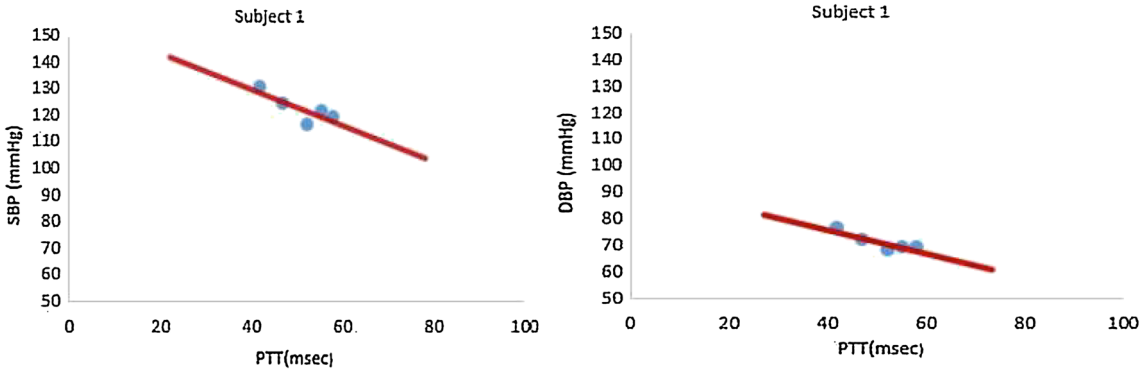

Fig. 8 Correlation scatter plots with the linear regression

AGM has better correlation with BP than not using AGM, which means that adjusting PTT using AGM is necessary in rPPG signal.

4.4 PTT–BP relation

We use VideoBP dataset for evaluating the proposed BP estimation method. Correlation between BP (SBP and DBP) and PTT for each subject is described in Table 2. The average inter-person coefficient of correlation between SBP and PTT is -0.840 ± 0.11, while correlation between DBP and PTT is -0.666 ± 0.10. Correlation scatter plots with the linear regression line for subject 1 are represented in Fig. 8. From the Table 2, we can see PTT have a slight variation over different subjects, and each subject has a relatively stable PTT range. This may be caused by the vessel distribution. From the observation of experiment, we found that the location of selected pairs from local regions of same subjects is much more stable during different visits, leading to a more stable PTT value.

To evaluate the performance of proposed BP estimation method, we use mean absolute difference (MAD) and standard difference (SD), respectively. MAD is a measure of the bias of BP estimates, while SD is a measure of error variability. Table 3 summarizes the values of MAD and SD of our proposed method for BP estimation. The results show that this foundation study to estimate SBP and DBP using a camera needs further research for successful real-life application.

5 Conclusion

Pulse transit time highly correlates with BP, which can be used for the BP estimation. Some studies have shown the PTT can be estimated from two PPG signals (i.e., cPPG

Table 3 Performance of proposed method for BP estimation

	SBP	DBP
1	5.3	1.13
2	2.76	16.6
3	9.66	7.48
4	21.6	14.8
5	5.53	16.49
6	16.25	19.8
MAD	8.42	12.34
SD	8.81	7.10

and rPPG). Due to the natural characteristics of rPPG, the dicrotic notch of rPPG signal often disappears and it is hard to be detected, which causes the problem of peak shifting. The PTT as well as BP estimation are thus influenced. In this paper, an adaptive Gaussian model is developed for secondary peak detection. The PTT estimation can be improved using the proposed model. The relationship between PTT and BP are then analyzed. Experimental results show there is a better relation between improve PTT and BP. Also, this result shows the disappearance of the secondary peak in rPPG waveform affects the PTT estimation, which may further affect BP estimation. The improved PTT using the proposed curve fitting method could reduce this influence and result in a more accurate BP. Further investigation will be conducted to improve the accuracy of PTT and BP.

References

Baltrušitis T, Robinson P, Morency L-P (2016) Openface: an open source facial behavior analysis toolkit. In: IEEE winter conference on applications of computer vision, pp 1–10

De Haan G, Jeanne V (2013) Robust pulse rate from chrominance-based rppg. IEEE Trans Biomed Eng 60:2878–2886

Drzewiecki G, Hood R, Apple H (1994) Theory of the oscillometric maximum and the systolic and diastolic detection ratios. Ann Biomed Eng 22(1):88–96

Gesche H, Grosskurth D, Kuchler G, Patzak A (2012) Continuous blood pressure measurement by using the pulse transit time: comparison to a cuff-based method. Eur J Appl Physiol 112(1):309–315

Haque MA, Irani R, Nasrollahi K, Moeslund TB (2016) Heartbeat rate measurement from facial video. IEEE Intell Syst 31(3):40–48

Hassan MA et al (2017) Heart rate estimation using facial video: a review. Biomed Signal Process Control 38:346–360

Henriques JF, Caseiro R, Martins P, Batista J (2015) High speed tracking with kernelized correlation filters. IEEE Trans Pattern Anal Mach Intell 37(3):583–596

Hsu GS, Ambikapathi A, Chen MS (2017) Deep learning with time-frequency representation for pulse estimation from facial videos. In: Biometrics (IJCB), 2017 IEEE international joint conference, pp 383–389

Jeong IC, Finkelstein J (2012) Interactive biking exercise (ibike) platform to facilitate lower extremity cycling exercise: system design and feasibility. In: Biomedical engineering and informatics (BMEI), 2012 5th international conference, pp 1091–1095

Jeong IC, Finkelstein J (2016) Introducing contactless blood pressure assessment using a high speed video camera. J Med Syst 40(4):77

Kumar M, Veeraraghavan A, Sabharwal A (2015) Distance PPG: Robust non-contact vital signs monitoring using a camera. Biomed Opt Express 6(5):1565–1588

Lewandowska M, Rumiński J, Kocejko T, Nowak J (2011) Measuring pulse rate with a web camera non-contact method for evaluating cardiac activity. In: Computer science and information systems (FedCSIS), federated conference, pp 405–410

Li X, Chen J, Zhao G, Pietikainen M (2014) Remote heart rate measurement from face videos under realistic situations. In: Proceedings of the IEEE conference on computer vision and pattern recognition, pp 4264–4271

Ma T, Zhang Y (2005) A correlation study on the variabilities in pulse transit time, blood pressure, and heart rate recorded simultaneously from healthy subjects. In: IEEE-EMBS, pp 996–999

Malasinghe LP, Ramzan N, Dahal K (2017) Remote patient monitoring: a comprehensive study. J Ambient Intell Hum Comput. https://doi.org/10.1007/s12652-017-0598-x

Martín-Martínez D, Casaseca-de-la Higuera P, Martín- Fernaídez M, Alberola-López C (2013) Stochastic modelling of the ppg signal: a synthesis-by-analysis approach with applications. IEEE Trans Biomed Eng 60(9):2432–2441

Mukkamala R, Hahn J-O, Inan OT, Mestha LK, Kim C-S, Toreyin H, Kyal S (2015) Toward ubiquitous blood pressure monitoring via pulse transit time: theory and practice. IEEE Trans Biomed Eng 62(8):1879– 1901

Patzak A, Mendoza Y, Gesche H, Konermann M (2015) Continuous blood pressure measurement using the pulse transit time: comparison to intra-arterial measurement. Blood Press 24(4):217–221

Poh M-Z, McDuff DJ, Picard RW (2010) Non-contact, automated cardiac pulse measurements using video imaging and blind source separation. Opt Express 18(10):762–774

Rubins U (2008) Finger and ear photoplethysmogram waveform analysis by fitting with gaussians. Med Biol Eng Comput 46(12):1271–1276

Sathyanarayana S, Satzoda R, Sathyanarayana S, Thambupillai S (2018) Vision-based patient monitoring: a comprehensive review of algorithms and technologies. J Ambient Intell Hum Comput 9(2):225–225

Shao D, Yang Y, Liu C, Tsow F, Yu H, Tao N (2014) Non-contact monitoring breathing pattern, exhalation flow rate and pulse transit time. IEEE Trans Biomed Eng 61(11):2760–2767

Smith RP, Argod J, Pépin J-L, Levy PA (1999) Pulse transit time: an appraisal of potential clinical applications. Thorax 54(5):452–457

Tasli HE, Gudi A, Uyl M (2014) Remote ppg based vital sign measurement using adaptive facial regions. In: Image processing (ICIP), 2014 IEEE international conference, pp 1410–1414

Tulyakov S, Alameda-Pineda X, Ricci E, Yin L, Cohn JF, Sebe N (2016) Self-adaptive matrix completion for heart rate estimation from face videos under realistic conditions. In: Proceedings of the IEEE conference on computer vision and pattern recognition, pp 2396–2404

Vanderpohl IJ III (2014) Measuring multiple physiological parameters through blind signal processing of video parameters. US Patent App. 14/202, 567

Verkruysse W, Svaasand LO, Nelson JS (2008) Remote plethysmographic imaging using ambient light. Opt Express 16(26):21434–21445

Yoon Y, Cho JH, Yoon G (2009) Non-constrained blood pressure monitoring using ecg and ppg for personal health care. J Med Syst 33(4):261–266